Geometry-Calibrated DRO: Combating Over-Pessimism with Free Energy Implications

Jiashuo Liu [1 *] **Jiayun Wu** [1 *] **Tianyu Wang** [2] **Hao Zou** [3] **Bo Li** [4] **Peng Cui** [1]

Abstract

Machine learning algorithms minimizing average risk are susceptible to distributional shifts. Distributionally Robust Optimization (DRO) addresses this issue by optimizing the worst-case risk within an uncertainty set. However, DRO suffers from over-pessimism, leading to low-confidence predictions, poor parameter estimations as well as poor generalization. In this work, we conduct a theoretical analysis of a probable root cause of over-pessimism: excessive focus on noisy samples. To alleviate the impact of noise, we incorporate data geometry into calibration terms in DRO, resulting in our novel Geometry-Calibrated DRO (GCDRO) for regression. We establish the connection between our risk objective and the Helmholtz free energy in statistical physics, and this free-energy-based risk can extend to standard DRO methods. Leveraging gradient flow in Wasserstein space, we develop an approximate minimax optimization algorithm with a bounded error ratio and elucidate how our approach mitigates noisy sample effects. Comprehensive experiments confirm GCDRO's superiority over conventional DRO methods.

1. Introduction

Machine learning algorithms with empirical risk minimization (ERM) have been shown to perform poorly under distribution shifts, especially sub-population shifts where substantial data subsets are underrepresented in the average risk due to their small sample sizes. As an alternative, Distributionally Robust Optimization (DRO) (Namkoong & Duchi, 2017; Blanchet & Murthy, 2019; Liu et al., 2022a; Gao & Kleywegt, 2022; Gao et al., 2022) aims to optimize against the worst-case risk distribution within a predefined uncertainty set. This uncertainty set is centered around the training distribution, and generalization performance can be guaranteed when the test distribution falls within this set.

However, DRO methods have been found to experience the over-pessimism problem in practice (Hu et al., 2018; Zhai et al., 2021) (*i.e.*, low-confidence predictions, poor parameter estimations, and generalization). Recent studies have sought to address this issue. From the *uncertainty set perspective*, Blanchet et al. (2019b); Liu et al. (2022a;b) proposed data-driven methods to learn distance metrics from data. However, these approaches remain vulnerable to noisy samples, as demonstrated in Table 2. Recently, Słowik & Bottou (2022); Agarwal & Zhang (2022) observed that DRO may overly focus on sub-populations with higher noise levels, leading to suboptimal generalization. Consequently, from the *risk objective perspective*, they suggest incorporating calibration terms to mitigate this issue. Nevertheless, applicable calibration terms either require expert knowledge or are computationally intensive, and few practical algorithms have been proposed.

To devise a practical calibration term for DRO, we first aim to identify the root causes of over-pessimism, which we attribute to the excessive focus on noisy samples that frequently exhibit higher prediction errors. For typical DRO methods (Namkoong & Duchi, 2017; Staib & Jegelka, 2019; Duchi & Namkoong, 2021; Liu et al., 2022b), based on a simple yet insightful linear example, we theoretically demonstrate that the variance of estimated parameters becomes substantially large when noisy samples have higher densities, in line with the empirical findings reported in (Zhai et al., 2021). Furthermore, we demonstrate that existing outlier-robust regression methods are not directly applicable for mitigating noisy samples in DRO scenarios where both noisy samples and distribution shifts coexist, highlighting the non-trivial nature of this problem.

In this work, inspired by the ideas in (Słowik & Bottou, 2022; Agarwal & Zhang, 2022), we design calibration terms, $i.e.$, total variation and entropy regularization, to prevent DRO from excessively focusing on random noisy samples. In conjunction with the Geometric Wasserstein uncertainty

[*]Equal contribution [1]Department of Computer Science and Technology, Tsinghua University [2]Department of Industrial Engineering and Operations Research, Columbia University [3]Zhongguancun Lab [4]School of Economics and Management, Tsinghua University. Correspondence to: Jiashuo Liu <liujiashuo77@gmail.com>, Peng Cui <cuip@tsinghua.edu.cn>.

Proceedings of the 41st International Conference on Machine Learning, Vienna, Austria. PMLR 235, 2024. Copyright 2024 by the author(s).

set (Liu et al., 2022b) utilized in our methods, these calibration terms effectively incorporate information from the data manifold, leading to improved regulation of the worst-case distribution in DRO. Specifically, during the optimization, the total variation term penalizes the variation of weighted prediction errors along the data manifold, preventing random noisy samples from gaining excessive densities. The entropy regularization term, also used in (Liu et al., 2022b), acts as a non-linear graph Laplacian operator that enforces the smoothness of the sample weights along the manifold. These calibration terms work together to render the worst-case distribution more *reasonable* for DRO, leading to our Geometry-Calibrated DRO (GCDRO) approach. We validate the effectiveness of our GCDRO on both simulation and real-world data.

Furthermore, from a statistical physics perspective, we demonstrate that our risk objective corresponds to the Helmholtz free energy, comprising three components: interaction energy, potential energy, and entropy. The free energy formulation generalizes typical DRO methods such as KL-DRO (Hu & Hong, 2013), χ^2-DRO (Duchi & Namkoong, 2021), MMD-DRO (Staib & Jegelka, 2019) and GDRO (Liu et al., 2022b). This physical interpretation provides a novel perspective for understanding different DRO methods by drawing parallels between the worst-case distribution and the steady state in statistical physics, offering valuable insights. From the free energy point of view, our GCDRO *specifically addresses the interaction energy between samples to mitigate the effects of noisy samples*. Motivated by the study of the Fokker-Planck equation (FPE, Chow et al. (2017); Esposito et al. (2021)), through gradient flow in the Geometric Wasserstein space, we derive an approximate minimax algorithm with a bounded error ratio $e^{-CT_{in}}$ after T_{in} inner-loop iterations. Our optimization method supports any quadratic form of interaction energy, potentially paving the way for designing more effective calibration terms for DRO in the future.

2. Preliminaries: Noisy Samples Bring Over-Pessimism in DRO

Notations. $X \in \mathcal{X}$ denotes the covariates, $Y \in \mathcal{Y}$ denotes the target, $f_\theta(\cdot) : \mathcal{X} \to \mathcal{Y}$ is the predictor parameterized by $\theta \in \Theta$. $\hat{P}_N$ denotes the empirical counterpart of distribution $P(X, Y)$ with N samples, and $\mathbf{p} = (p_1, \ldots, p_N)^T \in \mathbb{R}_+^N$ is the probability vector. $[N] = \{1, 2, \ldots, N\}$ denotes the set of integers from 1 to N. The random variable of data points is denoted by $Z = (X, Y) \in \mathcal{Z}$. The random vector of n dimension is denoted by $\vec{h}_n = (h_1, \ldots, h_n)^T$. We use δ_x to represent Dirac measure on the single point x. $G_N = (V, E, W)$ denotes a finite weighted graph with N nodes, where $V = [N]$ is the vertex set, E is the edge set and $W = \{w_{ij}\}_{(i,j)\in E}$ is the weight matrix of the graph. And $(x)_+ = \max(x, 0)$.

Distributionally Robust Optimization (DRO) is formulated as:

$$\theta^*(P) = \arg\min_{\theta\in\Theta} \sup_{Q\in\mathcal{P}(P)} \mathbb{E}_Q[\ell(f_\theta(X), Y)] \tag{1}$$

where ℓ is the loss function (typically mean square error) and $\mathcal{P}(P) = \{Q : \text{Dist}(Q, P) \le \rho\}$ denotes the ρ-radius uncertainty ball around the distribution P. Different distance metrics derive different DRO methods, e.g., f-divergence DRO (f-DRO, Ben-Tal et al. (2013)) with the Cressie-Read family of Rényi divergence, Wasserstein DRO (WDRO, Sinha et al. (2018); Blanchet & Murthy (2019); Blanchet et al. (2019a;b)), MMD-DRO (Staib & Jegelka, 2019) with maximum mean discrepancy, Geometric DRO (GDRO, Liu et al. (2022b)) with Geometric Wasserstein distance, and some refined distance metrics recently (Wang et al., 2021; Blanchet et al., 2023). Although DRO methods are designed to resist sub-population shifts, they have been observed to have poor generalization performances statistically (Słowik & Bottou, 2022; Zeng & Lam, 2022; Iyengar et al., 2023) and empirically (Hu et al., 2018; Frogner et al., 2019), which is referred to as over-pessimism.

In this section, we identify one of the root causes of the over-pessimism of DRO: the *excessive focus on noisy samples with typically high prediction errors*.

- We showcase DRO methods' excessive focus on noisy samples in practice and reveal their probability densities are linked to high prediction errors in worst-case distributions.
- Through a simple yet insightful regression example, we prove that such a phenomenon leads to high estimation variances and subsequently poor generalization performance.
- We demonstrate that existing outlier-robust regression methods are not directly applicable for mitigating noisy samples in DRO scenarios, emphasizing the non-trivial nature of this problem.

Problem Setting Given the *underlying* clean distribution $P_{\text{clean}} = (1-\alpha)P_{\text{major}} + \alpha P_{\text{minor}}, 0 < \alpha < \frac{1}{2}$, the goal of DRO can be viewed as achieving good performance across all possible sub-populations P_{minor}. Denote the observed contaminated training distribution by P_{train}. Based on Huber's ϵ-contamination model (Huber, 1992), we formulate P_{train} as:

$$P_{\text{train}} = (1-\epsilon)P_{\text{clean}} + \epsilon\tilde{Q} = \underbrace{(1-\epsilon)(1-\alpha)P_{\text{major}}}_{\text{major sub-population}} + \underbrace{(1-\epsilon)\alpha P_{\text{minor}}}_{\text{minor sub-population}} + \underbrace{\epsilon\tilde{Q}}_{\text{noisy sub-population}},$$

where $\tilde{Q}$ is an arbitrary *noisy* distribution (typically with larger noise scale), $0 < \epsilon < \frac{1}{2}$ is the noise level. Note that the *minor sub-population could represent any distribution*

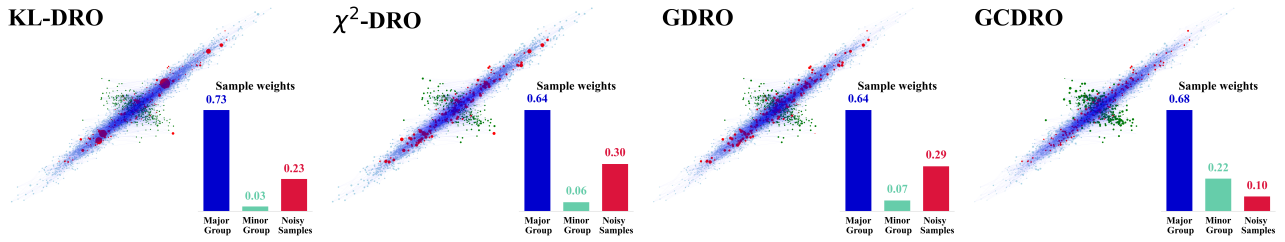

Figure 1: Visualizing the Worst-Case Distribution for Different DRO Methods: We show the data manifold and sample weights for each point, where blue points represent the major group, green ones represent the minor group, and red ones are noisy samples. The bars display the total sample weights of different groups, and the *original* group ratio is major (**93.1%**), minor (**4.9%**), noisy (**2%**).

with a proportion of α *in* P. However, we explicitly specify it here to emphasize the distinction between our setting and the traditional Huber's ϵ-contaminated setting, as the latter does *not* take sub-population shifts into account.

This corresponds with *real scenarios* where (1) different sub-populations (e.g., demographic groups or data sources) and (2) noisy samples (e.g., measurement errors, data collection errors) coexist. We expect a perfect DRO algorithm should achieve consistent performance across P_{major} and P_{minor} while unaffected by the noise from $\tilde{Q}$. This is a typical problem setting in DRO literature (Duchi & Namkoong, 2021; Zhai et al., 2021).

Empirical Observations. Following a typical regression setting (Duchi & Namkoong, 2021; Liu et al., 2022b), we demonstrate the worst-case distribution of KL-DRO, χ^2-DRO, and GDRO in Figure 1, where the size of each point is proportional to its density. In this scenario, the underlying distribution P comprises a known major sub-population (95%, blue points) and a minor sub-population (5%, green points). And the noise level ϵ in P_{train} is 2%. DRO methods are expected to upweight samples from minor sub-population to learn a model with uniform performances w.r.t. sub-populations. However, from Figure 1, we could observe that KL-DRO, χ^2-DRO and GDRO excessively focus on noisy samples, resulting in a noise level 10 to 15 times larger than the original. This observation helps to explain their poor performance on this task (detailed results can be found in Table 2).

Theoretical Analysis. To support our observations, we first analyze the worst distribution of KL-DRO, χ^2-DRO and GDRO, shedding light on the underlying reasons for this phenomenon.

Proposition 2.1 (Worst-case Distribution)**.** *Denote the worst-case distribution* $\widehat{Q}_N^*$ *as:*

$$\widehat{Q}_N^* := \arg \sup_{Q \in \mathcal{P}(\hat{P}_N)} \sum_{i=1}^{N} q_i \ell(f_\theta(x_i), y_i), \tag{2}$$

For different choices of Dist$(\cdot,\cdot)$ *in* $\mathcal{P}(P) = \{Q : \textit{Dist}(Q,P) \le \rho\}$*, we have* $\widehat{Q}_N^* = \sum_{i\in[N]} q_i^* \delta_{(x_i,y_i)}$*. Denote* $\ell(f_\theta(x_i), y_i)$ (abbr. ℓ_i) *as the prediction error of sample* $i \in [N]$*, we have:*

- *KL-DRO:* $q_i^*/q_j^* \propto \exp\left(\frac{\ell_i - \ell_j}{\eta}\right)$*, and* $\eta > 0$ *is the dual parameter;*
- *GDRO's final state (gradient flow step* $T \to \infty$*):* $q_i^*/q_j^* \propto \exp\left(\frac{\ell_i - \ell_j}{\eta}\right)$*, and* $\eta > 0$ *is the dual parameter;*
- χ^2*-DRO:* $q_i^*/q_j^* = (\ell_i - \lambda)_+/(\ell_j - \lambda)_+$*, and* $\lambda \ge 0$ *is the dual parameter.*

Proposition 2.1 demonstrates that for KL-DRO, χ^2-DRO, and GDRO (large gradient flow step), the *relative density* between samples is solely determined by their prediction errors, indicating that a larger prediction error results in a higher density. However, in our problem setting, samples from *both* minor sub-population P_{minor} *and* noisy sub-population $\tilde{Q}$ exhibit high prediction errors. The primary goal of DRO is to focus on the minor sub-population P_{minor}, but the presence of noisy samples in $\tilde{Q}$ significantly interferes with this objective and hurts model learning. As shown in Figure 1, for KL-DRO, χ^2-DRO and GDRO, noisy samples attract much density. Intuitively, it is not surprising that an excessive focus on noisy samples can have a detrimental impact. As KL-DRO, χ^2-DRO, and GDRO can be viewed as optimization within a weighted empirical distribution, we use the following simple example with the weighted least square model to demonstrate how this excessive focus on noisy samples can lead to high estimation variance, ultimately causing over-pessimism.

Example (Weighted Least Square)**.** Consider the data generation process as $Y = kX + \xi$, where $X, Y \in \mathbb{R}$ and random noise ξ satisfies $\xi \perp X$, $\mathbb{E}[\xi] = 0$ and $\mathbb{E}[\xi^2]$ (*abbr.* σ^2) is finite. Assume that the training dataset X_D consists of clean samples $\{x_c^{(i)}, y_c^{(i)}\}_{i\in[N_c]}$ and noisy samples $\{x_o^{(i)}, y_o^{(i)}\}_{i\in[N_o]}$ with $\sigma_c^2 < \sigma_o^2$. Consider the weighted least-square model $f(X) = \theta X$. Denote the sample weight of a clean sample $(x_c^{(i)}, y_c^{(i)})$ as $w_c^{(i)} \in \mathbb{R}_+, i \in [N_c]$,

and the sample weight of a noisy sample $(x_o^{(i)}, y_o^{(i)})$ as $w_o^{(i)} \in \mathbb{R}_+, i \in [N_o]$ with $\sum_{i\in[N_c]} w_c^{(i)} + \sum_{i\in[N_o]} w_o^{(i)} = 1$. Given the fixed covariates in the dataset $X_D = \{x_c^{(i)}\}_1^{N_c} \cup \{x_o^{(i)}\}_1^{N_o}$, the variance of the estimator $\hat{\theta}$ is given by:

$$\mathrm{Var}[\hat{\theta}|X_D] = \frac{\sum_{i=1}^{N_c}(w_c^{(i)})^2(x_c^{(i)})^2\sigma_c^2 + \sum_{i=1}^{N_o}(w_o^{(i)})^2(x_o^{(i)})^2\sigma_o^2}{\left[\sum_{i=1}^{N_c} w_c^{(i)}(x_c^{(i)})^2 + \sum_{i=1}^{N_o} w_o^{(i)}(x_o^{(i)})^2\right]^2},$$

where the minimum variance above is achieved if and only if $w_o^{(j)}/w_c^{(i)} = \sigma_c^2/\sigma_o^2 < 1, \forall i \in [N_c], j \in [N_o]$.

From the results, we make the following remarks:

• If noisy samples have higher weights than clean samples (e.g., $w_o/w_c > 1$), the variance of the estimated parameter $\hat{\theta}$ will be larger, suggesting that the learned $\hat{\theta}$ could be significantly unstable.

• In conjunction with Proposition 2.1, DRO methods tend to assign high weights to noisy samples, which can lead to unstable parameter estimation. While this example is relatively simple, this phenomenon aligns with the empirical findings in Zhai et al. (2021), which demonstrate that DRO methods can be quite unstable when confronted with label noise. Furthermore, directly analyzing the effect of noisy samples remains an open problem in the field of DRO.

Relationship with conventional outlier-robust regression. We would like to explain why conventional outlier-robust regression methods cannot be directly applied to our problem. The main challenge stems from the *coexistence* of noisy samples and minor sub-populations, both of which typically exhibit high prediction errors, leading to a misleading worst-case distribution in DRO. Conventional outlier-robust regression methods (Diakonikolas & Kane, 2018; Klivans et al., 2018; Diakonikolas et al., 2022) primarily focus on mitigating the effects of outliers without considering sub-population shifts. As a result, these methods are not directly applicable in this context. For instance, the L_2-estimation-error of outlier-robust linear regression is $\mathcal{O}(\epsilon \log(1/\epsilon))$ (Diakonikolas & Kane, 2018), where ϵ represents the noise level in Equation 1. However, as analyzed in Proposition 2.1 and demonstrated in Figure 1, during the optimization of DRO, the noise level ϵ significantly increases, rendering even outlier-robust estimation quite inaccurate. Moreover, Klivans et al. (2018) propose finding a pseudo distribution with minimal prediction errors to avoid outliers (see Algorithm 5.2 in Klivans et al. (2018)). Nevertheless, this approach might inadvertently exclude minor sub-populations, which should be the focus under sub-population shifts, due to the main challenge: the *coexistence* of noisy samples and minor sub-populations. Zhai et al. (2021) incorporate this idea into DRO. Still, their method requires an implicit assumption that the prediction errors of noisy samples are higher than those of minor sub-populations, which does not always hold in practice. And Bennouna & Van Parys (2022) build the uncertainty set via two measures, KL-divergence and Wasserstein distance, leading to a combined approach of KL-DRO and ridge regression. Despite this, as we discussed earlier, DRO tends to increase the noise level in data, making it difficult to fix using ridge regression.

Based on the analysis above, we stress the importance of integrating more information from data. In pursuit of this, we propose to leverage the unique geometric properties that distinguish noisy samples from minor sub-populations to address this issue.

3. Proposed Method

In this work, with a focus on regression, we introduce our Geometry-Calibrated DRO (GCDRO). The fundamental idea is to utilize data geometry to distinguish between random noisy samples and minor sub-populations. It is motivated by the fact that prediction errors for minor sub-populations typically exhibit local smoothness along the data manifold, a property that is not shared by noisy samples.

Discrete Geometric Wasserstein Distance. We briefly revisit the definition of the discrete geometric Wasserstein distance. Given a weighted finite graph $G_N = (V, E, W)$, the probability set $\mathscr{P}(G_N)$ supported on the vertex set V is defined as $\mathscr{P}(G_N) = \{\mathbf{p} \in \mathbb{R}^N | \sum_{i=1}^N p_i = 1, p_i \geq 0, \text{for } i \in V\}$, and its interior is denoted as $\mathscr{P}_o(G_N)$. A velocity field $\mathbf{v} = (v_{ij})_{i,j\in V} \in \mathbb{R}^{N\times N}$ on G_N is defined on the edge set E satisfying that $v_{ij} = -v_{ji}$ if $(i,j) \in E$. $\xi_{ij}(\mathbf{p})$ is a function interpolated with the associated nodes' densities p_i, p_j. The flux function $\mathbf{pv} \in \mathbb{R}^{N\times N}$ on G_N is defined as $\mathbf{pv} := (v_{ij}\xi_{ij}(\mathbf{p}))_{(i,j)\in E}$ and its divergence is defined as $\mathrm{div}_{G_N}(\mathbf{pv}) := -(\sum_{j\in V:(i,j)\in E} \sqrt{w_{ij}} v_{ij}\xi_{ij}(\mathbf{p}))_{i=1}^N \in \mathbb{R}^N$. Then for distributions $\mathbf{p}_0, \mathbf{p}_1 \in \mathscr{P}_o(G_N)$, the discrete geometric Wasserstein distance (Chow et al., 2017; Liu et al., 2022b) is defined as:

$$\mathcal{GW}^2_{G_N}(\mathbf{p}_0, \mathbf{p}_1) := \inf_v \left\{ \int_0^1 \frac{1}{2} \sum_{(i,j)\in E} \xi_{ij}(\mathbf{p}(t)) v_{ij}^2 dt \right.$$
$$\left. \text{s.t.} \frac{d\mathbf{p}}{dt} + \mathrm{div}_{G_N}(\mathbf{pv}) = 0, \mathbf{p}(0) = \mathbf{p}_0, \mathbf{p}(1) = \mathbf{p}_1 \right\}. \tag{3}$$

Equation 3 computes the shortest (geodesic) length among all potential plans, integrating the total kinetic energy of the velocity field throughout the transportation process. A key distinction from the Wasserstein distance is that it only permits density to appear at the graph nodes.

Formulation Given training dataset $D_{tr} = \{(x_i, y_i)\}_{i=1}^N$ and a finite weighted graph $G_N = (V, E, W)$ representing the inherent structure of sample covariates. Denote the empirical marginal distribution as $\hat{P}_X$, the formulation of

GCDRO is:

$$\min_{\theta\in\Theta} \underbrace{\sup_{\mathbf{q}:\mathcal{GW}^2_{G_N}(\hat{P}_X,\mathbf{q})\le\rho}}_{\text{Geometric Wasserstein set}} \Bigg\{\mathcal{R}_N(\theta,\mathbf{q}) := \sum_{i=1}^N q_i\ell(f_\theta(x_i),y_i) - \underbrace{\frac{\alpha}{2}\cdot\sum_{(i,j)\in E} w_{ij}q_iq_j(\ell_i-\ell_j)^2}_{\text{Calibration Term I}} - \underbrace{\beta\cdot\sum_{i=1}^N q_i\log q_i}_{\text{Calibration Term II}}\Bigg\}, \tag{4}$$

where ρ is the pre-defined radius of the uncertainty set, ℓ_i is the loss on the i-th sample and $w_{ij}\in W$ denotes the edge weight between sample i and j. α and β are hyper-parameters.

Illustrations. In our formulation, for any distribution $\mathbf{q}$ within the uncertainty set,
Calibration term I $\sum_{(i,j)\in E} w_{ij}q_iq_j(\ell_i-\ell_j)^2$ calculates the *graph total variation* of prediction errors along the data manifold that is characterized by G_N. Intuitively, when *selecting the worst-case distribution*, this term imposes a penalty on distributions that allocate high densities to random noisy samples, as this allocation significantly amplifies the overall variation in prediction errors. Conversely, this term does not penalize distributions that allocate high densities to minor sub-populations, as their errors are smooth and have a relatively small impact on the total variation along the manifold. This differing phenomenon arises from the distinct geometric properties of random noisy samples and minor sub-populations, as samples from the latter typically cluster together on the data manifold. Further, *during the optimization of model parameter* θ, this term acts like a variance term, resulting in a quantile-like risk objective, which helps to mitigate the effects of outliers.
Calibration term II $\sum_{i=1}^N q_i\log q_i$ represents the negative entropy of distribution $\mathbf{q}$. As discussed in Section 3.2, during optimization, this term transforms into a non-linear *graph Laplacian operator* that encourages sample weights to be smooth along the manifold, avoiding extreme sample weights in the worst-case distribution.

3.1. Free Energy Implications on Worst-case Distribution

We first demonstrate the free energy implications of our risk objective $\mathcal{R}_N(\theta,\mathbf{q})$. Intuitively, the change of sample weights across N samples (the inner maximization problem of $\mathcal{R}_N(\theta,\mathbf{q})$) can be analogously related to the dynamics of particles in a system, wherein the concentration of densities coincides with the aggregation of particle masses at N distinct locations (in the case of infinite samples, these locations converge to the data manifold). As a result, a deeper understanding of the steady state in a particle system can offer *valuable insights into the worst-case distribution* for DRO.

Building on this analogy, we can dive deeper into the physics of particle interactions. When particles exist within a potential energy field, they are subject to external forces. Simultaneously, there are interactions among the particles themselves, leading to a constant state of motion within the system. In statistical physics, a key point of interest is identifying when a system reaches a steady state. In a standard process like the reversible isothermal process, it is established that spontaneous reactions consistently move in the direction of decreasing *Helmholtz free energy* (Fu et al., 1990; Reichl, 1999; Friston, 2010), which consists of interaction energy, potential energy and the negative entropy:

$$\begin{aligned}\mathcal{E}(\mathbf{q}) &= \underbrace{\mathbf{q}^\top K\mathbf{q}}_{\text{Interaction Energy}} + \underbrace{\mathbf{q}^\top V}_{\text{Potential Energy}} - \underbrace{\beta\sum_{i=1}^N(-q_i\log q_i)}_{\text{Temperature}\times\text{Entropy}} \\ &= -\mathcal{R}_N(\theta,\mathbf{q}).\end{aligned} \tag{5}$$

By taking $V=-\vec{\ell}$ and $K_{ij}=\frac{\alpha}{2}w_{ij}(\ell_i-\ell_j)^2$ for $(i,j)\in E$, our risk objective is a special case of Helmholtz free energy, where the potential energy of sample i is $-\ell_iq_i$ and the interaction energy between sample i and j is $\frac{\alpha}{2}w_{ij}(\ell_i-\ell_j)^2q_iq_j$. Specifically, such mutual interactions can manifest as *repulsive forces between adjacent particles*, thereby preventing the concentration of mass in locations where local prediction errors are significantly high. And this explains from a physical perspective why our calibration term **I** could mitigate random noisy samples.

Additionally, Proposition 3.1 offers physical interpretations to comprehend the worst-case distribution of various DRO methods. We make some remarks: (1) current DRO methodologies, except MMD-DRO, do not explicitly formulate the interaction term between samples in their design considerations (χ^2-DRO does not involve interaction between samples), despite the corresponding interaction energy between particles being a common phenomenon in physics; (2) MMD-DRO simply uses kernel gram matrix for interaction and lacks efficient optimization algorithms; (3) by *considering this interaction energy*, our proposed GCDRO is capable of mitigating the impacts of random noisy samples.

Proposition 3.1 (Free Energy Implications)**.** *The dual reformulations of some typical DRO methods are equivalent to the free-energy-based minimax problem* $\min_{\theta\in\Theta,\lambda\ge0}\max_{\mathbf{q}\in\mathscr{P}}\Big\{\lambda\rho - \mathcal{E}(\mathbf{q},\theta,\lambda)\Big\}$ *with different choices of* $\mathscr{P}$, ρ *and* $K, V, H[q]$ *in the free energy* $\mathcal{E}$. *Details are shown in Table 1.*

Through free energy, we could *understand* the type of energy or steady state that DRO methods strive to achieve, and design better interaction energy terms in DRO. Moreover,

Table 1: Free energy implications of some DRO methods. Δ_N denotes the N-dimensional simplex, η in marginal DRO is the dual parameter.

Method	Energy Type			Specific Formulation			
	Interaction	Potential	Entropy	K	V	$H[\mathbf{q}]$	$\mathscr{P}$
KL-DRO	✗	✔	✔	-	$-\vec{\ell}$	$H[\mathbf{q}]$	Δ_N
χ^2-DRO	✔	✔	✗	λI	$-\vec{\ell}$	-	Δ_N
MMD-DRO	✔	✔	✗	Kernel Gram Matrix K	$-\vec{\ell}-\frac{2\lambda}{N}K^\top\mathbf{1}$	-	Δ_N
Marginal χ^2-DRO	✗	✔	✗	-	$-(\vec{\ell}-\eta)_+$	-	Δ_N with Hölder continuity
GDRO	✗	✔	✔	-	$-\vec{\ell}$	$H[\mathbf{q}]$	Geometric Wasserstein Set
GCDRO	✔	✔	✔	Interaction Matrix K	$-\vec{\ell}$	$H[\mathbf{q}]$	Geometric Wasserstein Set

our optimization, as outlined in Section 3.2, could accommodate multiple quadratic forms of interaction energy.

3.2. Optimization

Then we derive an approximate minimax optimization for our GCDRO. For the *inner maximization* problem, we approximate it via the gradient flow of $-\mathcal{R}_N(\theta, Q)$ w.r.t. Q in the geometric Wasserstein space $(\mathscr{P}_o(G_N), \mathcal{GW}_{G_N})$. We show that the error rate is $\mathcal{O}(e^{-CT_{in}})$ after T_{in} iterations inner loop, which gives a nice approximation.

We denote the *continuous gradient flow* as $\mathbf{q} : [0, T] \to \mathscr{P}_o(G_N)$, the probability density of sample i at time t is abbreviated as $q_i(t)$, and the *time-discretized gradient flow* with time step τ as $\hat{\mathbf{q}}_\tau$. For inner maximization, we utilize the τ-time-discretized gradient flow (Villani, 2021) for $-\mathcal{R}_N(\theta, \mathbf{q})$ in the geometric Wasserstein space $(\mathscr{P}_o(G_N), \mathcal{GW}^2_{G_N})$ as:

$$\hat{\mathbf{q}}_\tau(t+\tau) = \underset{\mathbf{q}\in\mathscr{P}_o(G_N)}{\operatorname{argmax}} \ \mathcal{R}_N(\theta, \mathbf{q}) - \frac{1}{2\tau}\mathcal{GW}^2_{G_N}(\hat{\mathbf{q}}_\tau(t), \mathbf{q}). \tag{6}$$

The gradient of $\mathbf{q}$ in Equation 6 is given as (when $\tau \to 0$):

$$\frac{dq_i}{dt} = \sum_{(i,j)\in E} w_{ij}\xi_{ij}\Big(\mathbf{q},\ \ell_i - \ell_j + \beta(\log q_j - \log q_i) + \alpha\big(\sum_{h\in N(j)}(\ell_h-\ell_j)^2 w_{jh}q_h - \sum_{h\in N(i)}(\ell_h-\ell_i)^2 w_{ih}q_h\big)\Big), \tag{7}$$

where E is the edge set of G_N, w_{ij} is the edge weight between node i and j, $N(i)$ denotes the set of neighbors of node i, ℓ_i denotes the loss of sample i, and $\xi_{ij}(\cdot,\cdot) : \mathscr{P}(G_N) \times \mathbb{R} \to \mathbb{R}$ is:

$$\xi_{ij}(\mathbf{q}, v) := v \cdot \big(\mathbb{I}(v > 0)q_j + \mathbb{I}(v \le 0)q_i\big), v \in \mathbb{R},$$

which is the *upwind interpolation* commonly used in statistical physics and guarantees that the probability vector $\mathbf{q}$ keeps positive. From the gradient, we could see that the entropy regularization acts as a non-linear graph Laplacian operator to make the sample weights smooth along the manifold. Equation 7 is discretized via Forward Euler Method as:

$$q_i(t+\tau) = q_i(t) + \tau \cdot \frac{dq_i}{dt}, \tag{8}$$

where τ is the learning rate. In our algorithm, we fix the steps of the gradient flow to be T_{in} and prove that the error ratio is $e^{-CT_{in}}$ compared with the *ground-truth* worst-case risk $\mathcal{R}_N(\theta, \mathbf{q}^*)$ constrained in an $\rho(\theta, T_{in})$-radius ball.

Proposition 3.2 (Approximation Error Ratio)**.** *Given the model parameter θ, denote the distribution after time T_{in} as $\mathbf{q}^{T_{in}}(\theta)$, and the distance to training distribution $\hat{P}_X$ as $\rho(\theta, T_{in}) := \mathcal{GW}^2_{G_N}(\hat{P}_X, \mathbf{q}^{T_{in}}(\theta))$ (abbr. $\rho(\theta)$). Assume $\mathcal{R}_N(\theta, \mathbf{q})$ is convex w.r.t $\mathbf{q}$. Then define the ground-truth worst-case distribution $q^*(\theta)$ within the $\rho(\theta)$-radius ball as:*

$$\mathbf{q}^*(\theta) := \arg \sup_{\mathbf{q}:\mathcal{GW}^2_{G_N}(\hat{P}_X,\mathbf{q})\le\rho(\theta)} \mathcal{R}_N(\theta, \mathbf{q}).$$

The upper bound of the error rate of the objective function $\mathcal{R}_N(\theta, \mathbf{q}^{T_{in}})$ satisfies:

$$\frac{\mathcal{R}_N(\theta, \mathbf{q}^*) - \mathcal{R}_N(\theta, \mathbf{q}^{T_{in}})}{\mathcal{R}_N(\theta, \mathbf{q}^*) - \mathcal{R}_N(\theta, \hat{P}_X)} < e^{-CT_{in}},$$

$$C = 2m\lambda_{sec}(\hat{L})\lambda_{min}(\nabla^2\mathcal{R}_N)\frac{1}{(r+1)^2} > 0,$$

where $\hat{L}$ is the Laplacian matrix of G_N. $\lambda_{sec}, \lambda_{min}$ are the second smallest and smallest eigenvalue, m, r are constants depending on $\mathcal{R}_N, G_N, \beta$.

We make some remarks:

• For the assumption that $\mathcal{R}_N$ is convex w.r.t. $\mathbf{q}$, the Hessian is given by $\nabla^2\mathcal{R}_N = \beta\text{diag}(1/q_1, ..., 1/q_N) + 2K$. Since K is a sparse matrix whose nonzero elements in each row is far smaller than N, it is easily satisfied in empirical settings that the Hessian matrix $\nabla^2\mathcal{R}_N$ is diagonally dominant and thus positive definite, making the inner maximization concave w.r.t $\mathbf{q}$.

• During the optimization, our algorithm finds an approximately worst-case distribution that is close to the ground-truth one within a $\rho(\theta)$-radius uncertainty set. Our robustness guarantee is similar to Sinha et al. (2018) (see Equation 12 in Sinha et al. (2018)).
• The error ratio is $e^{-CT_{in}}$, enabling a nice approximation efficiently with finite T_{in} steps.

3.3. Mitigate the Effects of Random Noisy Samples

Finally, we prove that our GCDRO method effectively de-emphasizes 'noisy samples' with locally non-smooth prediction errors. Due to the challenge of assessing intermediate states in gradient flow, we focus on its final state (as $T_{in} \to \infty$).

For the worst-case distribution q^*, we denote the density ratio between samples as $\gamma(i,j) := q_i^*/q_j^*$. In sensitivity analysis, when *only* sample i is perturbed with label noises, we denote the density ratio in the new worst-case distribution $\tilde{q^*}$ as $\gamma^{\text{noisy}}(i,j) := \tilde{q_i^*}/\tilde{q_j^*}$. The sample weight sensitivity $\xi(i,j)$ is defined as $\xi(i,j) = \log\gamma^{\text{noisy}}(i,j) - \log\gamma(i,j)$, which measures how much density ratio changes under perturbations on one sample. Larger $\xi(i,j)$ indicates larger sensitivity to noisy samples.

Proposition 3.3. *Denote $N(i)$ as the set of neighbors of the i-th sample. Denote that $A = \sum_{k\in N(i)} \tilde{q}_k^* w_{ik}$, $B = \sum_{k\in N(i)} \tilde{q}_k^* w_{ik}(\ell_i - \ell_k)$, and $C = \sum_{k\in N(i)}(\tilde{q}_k^* - q_k^*)w_{ik}(\ell_i-\ell_k)^2 - \sum_{k\in N(j)}(\tilde{q}_k^* - q_k^*)w_{jk}(\ell_k-\ell_j)^2$.Denote the excess error induced by label noises on the i-th sample as $\delta = \ell_i^{noisy} - \ell_i$. When*

$$\delta \geq \delta_{min} := \begin{cases} -\frac{B}{A} + \sqrt{\left(\frac{B}{A}\right)^2 - \frac{C}{A}} & \text{if } B^2 - AC \geq 0, \\ 0, & \text{otherwise}. \end{cases}$$

For any $\alpha > 0$, we have $\xi_{GCDRO} < \xi_{GDRO}$. Furthermore, there exists $M > 0$ such that for any $\alpha > M$, we have $\xi_{GCDRO}(i,j) < 0 < \min\{\xi_{\chi^2-DRO}(i,j), \xi_{GDRO}(i,j)(= \xi_{KL\text{-}DRO}(i,j))\}$, indicating that GCDRO is not sensitive to locally non-smooth noisy samples.

Remark. Here we make some remarks: (a) B denotes the weighted average of the error gap in the neighborhood of the i-th sample; (b) Both terms in C represent the changes of local smoothness in the neightborhoods of the i-th and j-th samples respectively; (c) $-\frac{B}{A} = \frac{\sum_{k\in N(i)} \tilde{q}_k^* w_{ik}\ell_k}{\sum_{k\in N(i)} \tilde{q}_k^* w_{ik}} - \ell_i$ also captures the local smoothness. Specifically, it measure the gap between the weighted average error in the i-th sample's neighborhood and the error of sample i. Intuitively, smaller $|\frac{B}{A}|$ means a smoother neighborhood; (d) The form of M is $M = 1/(A\delta + 2B + \frac{C}{\delta}) \leq 1/(2\sqrt{AC} + 2B)$.

Relaxation of Proposition 3.3 We then proceed to relax the condition $\delta \geq \delta_{\text{min}}$ (to a looser condition) to give clearer insights on how it relates to the local smoothness. Denote

$$\delta_{\text{relax}} = \max_{k\in N(i)} |\ell_k - \ell_i| \cdot \left(1 + \sqrt{\sum_{t\in N(i)} w_{it}\frac{q_t^*}{\tilde{q}_t^*}}\right) > \delta_{\text{min}}, \tag{9}$$

and the condition could be simplified to: when $\delta \geq \delta_{\text{relax}}$, for any $\alpha > 0$, we have the above conclusion. This condition mainly relies on the local smoothness of the error within the i-th sample's neighborhood, which is measured by the maximal error gap between ℓ_i and its neighbors.

Implementation & Complexity. In practice, we do a grid search over $\alpha \in [0.1, 10]$ on an independent held-out validation dataset to select the best α. For our GCDRO, G_N is constructed as a k-nearest neighbor (kNN) graph from training data *once and for all* ***only at the initialization step***. For large-scale datasets, we use NN-Descent to estimate the kNN graph with an almost linear complexity of $\mathcal{O}(\mathbf{N^{1.14}})$. Since the sample weights are transferred along the edges of the graph, the simulation of gradient flow can be implemented similarly to message propagation with DGL package (Wang et al., 2019), which ***scales linearly with sample size*** and enjoys *parallelization by GPU*. The implementation above ensures the adaptability to large-scale data.

4. Experiments

In this section, we test the empirical performances of our proposed GCDRO on simulation data and real-world *regression* datasets with natural distribution shifts. As for the baselines, we compare with empirical risk minimization (ERM), WDRO, two typical f-DRO methods, including KL-DRO, χ^2-DRO (Duchi & Namkoong, 2021), GDRO (Liu et al., 2022b), HRDRO (Bennouna & Van Parys, 2022) and DORO (Zhai et al., 2021), where HRDRO and DORO are designed to mitigate label noises.

4.1. Simulation Data

Data Generation. We design simulation settings with both sub-population shifts and noisy samples. The input covariates $X = [S, U, V]^T \in \mathbb{R}^{10}$ consist of stable covariates $S \in \mathbb{R}^5$, irrelevant ones $U \in \mathbb{R}^4$ and the unstable covariate $V \in \mathbb{R}$:

$$\begin{aligned} &[S, U] \sim \mathcal{N}(0, 2\mathbb{I}_9), \varepsilon \sim N(0, 0.5), \\ &V \sim \text{Laplace}(\text{sign}(r)\cdot Y, 1/5\ln|r|) \\ &Y = \theta_S^T S + 0.1 S_1 S_2 S_3 + \varepsilon, \end{aligned}$$

where $\theta_S \in \mathbb{R}^5$ is the coefficients of the true model, $|r| > 1$ is the adjustment factor for each sub-population, and Laplace$(\cdot,\cdot)$ denotes the Laplace distribution. From the data generation, the relationship between S and Y stays invariant under different r, $U \perp Y$, while the relationship

Table 2: Results on the simulation data. We report the average root mean square errors (RMSE) over 5 runs, excluding the *small* standard deviations.

	Weak Label Noise (noise level 0.5%)					Strong Label Noise (noise level 5%)				
	Train (major)	Train (minor)	Test Mean	Test Std	Parameter Est Error	Train (major)	Train (minor)	Test Mean	Test Std	Parameter Est Error
ERM	0.337	0.850	0.598	0.264	0.423	0.368	0.855	0.599	0.243	0.431
WDRO	0.337	0.851	0.589	0.292	0.424	0.368	0.857	0.600	0.268	0.432
χ^2-DRO	0.596	0.765	0.680	0.088	0.447	1.072	0.708	0.875	0.193	0.443
KL-DRO	0.379	1.616	0.974	0.660	0.886	0.468	1.683	1.037	0.621	0.913
HRDRO	0.325	1.298	0.794	0.516	0.693	0.330	1.343	0.801	0.522	0.694
DORO	0.347	0.793	0.565	0.230	0.384	0.334	0.919	0.611	0.295	0.449
GDRO	0.692	0.516	0.605	0.094	0.198	0.618	0.752	0.677	0.063	0.421
GCDRO	0.411	0.554	**0.482**	**0.070**	**0.190**	0.494	0.591	**0.540**	**0.044**	**0.268**

between V and Y is controlled by r, which *varies across sub-populations*. Intuitively, $\text{sign}(r)$ controls whether the spurious correlation V-Y is positive or negative. And $|r|$ controls the strength of the spurious correlation: the larger $|r|$ is, the stronger the spurious correlation is. Furthermore, in order to conform to real data which are naturally assembled with label noises (Zhai et al., 2021), we introduce label noises by an ϵ proportion of labels as $Y' \sim \mathcal{N}(0, \text{Std}(Y))$. ϵ controls the noise level.

Settings. In training, we generate 9,500 points with $r = 1.9$ (*majority*, strong positive spurious correlation V-Y) and 500 points with $r = -1.3$ (*minority*, weak negative spurious correlation V-Y). In testing, we vary $r \in \{3.0, 2.3, -1.9, -2.7\}$ to simulate different spurious correlations V-Y. We use *linear model* with mean square error (MSE) and report the prediction root-mean-square errors (RMSE) for each sub-population, the mean and standard deviation of prediction errors among all testing sub-populations. Also, we report the parameter estimation errors $\|\hat{\theta} - \theta^*\|_2$ of all methods ($\theta^* = (\theta_S^T, 0, \ldots, 0)^T$). The results over 10 runs are shown in Table 2.

Analysis. From Table 2, Our proposed GCDRO outperforms all baselines under different strengths of label noises, which demonstrates its effectiveness. Compared with GDRO, we could see that our *calibration terms* in Equation 4 is effective to mitigate label noises. In contrast, compared with ERM, all typical DRO methods, especially χ^2-DRO and KL-DRO, are strongly affected by label noises. Besides, although DORO is designed to mitigate outliers, it does not perform well under strong noises ($\kappa = 5\%$), because it relies on the assumption that noisy points have the largest prediction errors, which does not always hold. Recall Figure 1, the worst-case distribution of our GCDRO *significantly upweighs on the minority* (green points) and does not put much density on the noisy data (red points), while the others put much higher weights on the noisy samples and perform poorly.

4.2. Real-world Data

We use three real-world regression datasets with natural distribution shifts, including bike-sharing prediction, house price, and temperature prediction. For all these experiments, we use a two-layer *MLP* model with mean square error (MSE). We use the Adam optimizer (Kingma & Ba, 2015) with the default learning rate $1e-3$. And all methods are trained for $5e3$ epochs. The hyper-parameter search space is specified in Appendix.

Datasets.

(1) **Bike-sharing** dataset (Dua & Graff, 2017) contains the daily count of rental bikes in the Capital bike-sharing system with the corresponding 11 weather and seasonal covariates. The task is to predict the count of rental bikes of *casual users*. Note that the count of casual users is likely to be more *random and noisy*, which is suitable to verify the effectiveness of our method. We split the dataset according to the season for natural shifts. In the training data, the ratio of four seasons' data is $9:7:5:3$. We test on the rest of the data and report the prediction error of each season.

(2) **House Price** dataset[1] contains house sales prices from King County, USA. The task is to predict the transaction price of the house via 17 predictive covariates such as the number of bedrooms, square footage of the house, etc. We divide the data into 5 sub-populations according to the built year of each house with each sub-population covering a span of 25 years. In training, we use data from the first group (built year < 1920) and report the prediction error for each testing group.

(3) **Temperature** dataset (Dua & Graff, 2017) is largely composed of the LDAPS model's next day's forecast data, in-situ maximum and minimum temperatures of present-day, and geographic auxiliary variables in South Korea from 2013 to 2017. The task is to predict the next-day's maximum air temperatures based on the 22 covariates. We divide

[1] https://www.kaggle.com/c/house-prices-advanced-regression- techniques/data

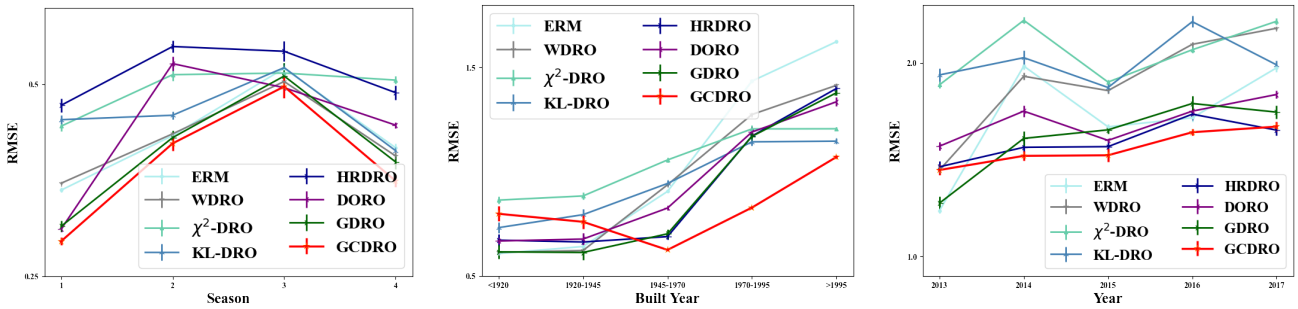

(a) **Bike-sharing** (b) **House Price** (c) **Temperature**

Figure 2: Results (over 5 runs) of real-world datasets with natural shifts. The average results and the standard deviations (error bars in the figure) are showed. Note that we do not manually add label noises here, since real-world datasets intrinsically contain noises.

the data into 5 groups corresponding with 5 years. In the training data, the ratio of five years' data is $9:7:5:3:1$. We test on the rest of the data and report the prediction error of each year. More details could be found in Appendix.

Analysis. From the results in Figure 2a, our proposed GCDRO outperforms all baselines under strong shifts, with the most stable performances under natural distribution shifts. In contrast, we could see that the performances of ERM drop a lot under distribution shifts, and DRO methods have better performance as well as robustness. Furthermore, in Appendix C, we visualize the learned manifold in Figure 3 and see that the learned kNN graph fits the data manifold well. We also show the performances of our GCDRO are relatively stable across different choices of k in Figure 4. In all, our GCDRO only needs the input graph G_N to represent the data structure and *any manifold learning or graph learning* methods could be plugged in to give a better estimation of G_N.

5. Future Directions

Our work deals with the over-pessimism in DRO via geometric calibration terms and provides free energy implications. The high-level idea could inspire future research on (1) relating free energy with DRO; (2) designing more reasonable calibration terms in DRO; (3) incorporating data geometry in general risk minimization algorithms. We hope this work could help to make DRO methods more effective in practice. And future improvements may be extend this method to classification scenarios with more complicated data like images and languages.

Acknowledgements

Peng Cui's research was supported in part by National Natural Science Foundation of China (No. 62141607). Bo Li's research was supported by the National Natural Science Foundation of China (No.72171131, 72133002); the Technology and Innovation Major Project of the Ministry of Science and Technology of China under Grants 2020AAA0108400 and 2020AAA0108403.

Impact Statement

The goal of this work is to address the over-pessimism problem in distributionally robust optimization (DRO). We introduce two calibration terms to further refine the uncertainty set, enabling the development of more realistic robust solutions. This work has the potential to significantly impact the design of DRO methods and improve the robustness and fairness of machine learning models. As machine learning models increasingly influence society, the framework presented in this paper represents a crucial step toward the trustworthy deployment of AI.

References

Agarwal, A. and Zhang, T. Minimax regret optimization for robust machine learning under distribution shift. *arXiv preprint arXiv:2202.05436*, 2022.

Belkin, M. and Niyogi, P. Laplacian eigenmaps for dimensionality reduction and data representation. *Neural Comput.*, 15(6):1373–1396, 2003. doi: 10.1162/089976603321780317. URL https://doi.org/10.1162/089976603321780317.

Ben-Tal, A., Den Hertog, D., De Waegenaere, A., Melenberg, B., and Rennen, G. Robust solutions of optimization problems affected by uncertain probabilities. *Management Science*, 59(2):341–357, 2013.

Bennouna, A. and Van Parys, B. Holistic robust data-driven decisions. *arXiv preprint arXiv:2207.09560*, 2022.

Blanchet, J. and Murthy, K. Quantifying distributional

model risk via optimal transport. *Mathematics of Operations Research*, 44(2):565–600, 2019.

Blanchet, J., Kang, Y., and Murthy, K. Robust wasserstein profile inference and applications to machine learning. *Journal of Applied Probability*, 56(3):830–857, 2019a.

Blanchet, J., Kuhn, D., Li, J., and Taskesen, B. Unifying distributionally robust optimization via optimal transport theory. *arXiv preprint arXiv:2308.05414*, 2023.

Blanchet, J. H., Kang, Y., Murthy, K. R. A., and Zhang, F. Data-driven optimal transport cost selection for distributionally robust optimization. In *2019 Winter Simulation Conference, WSC 2019, National Harbor, MD, USA, December 8-11, 2019*, pp. 3740–3751. IEEE, 2019b. doi: 10.1109/WSC40007.2019.9004785. URL https://doi.org/10.1109/WSC40007.2019.9004785.

Brown, B. C. A., Caterini, A. L., Ross, B. L., Cresswell, J. C., and Loaiza-Ganem, G. The union of manifolds hypothesis and its implications for deep generative modelling. *CoRR*, abs/2207.02862, 2022. doi: 10.48550/arXiv.2207.02862. URL https://doi.org/10.48550/arXiv.2207.02862.

Cacoullos, T. Estimation of a multivariate density. Technical report, University of Minnesota, 1964.

Chow, S.-N., Li, W., and Zhou, H. Entropy dissipation of fokker-planck equations on graphs. *arXiv preprint arXiv:1701.04841*, 2017.

Diakonikolas, I. and Kane, D. M. Algorithmic high-dimensional robust statistics. *Webpage http://www. iliasdiakonikolas. org/simons-tutorial-robust. html*, 2018.

Diakonikolas, I., Kane, D. M., Pensia, A., and Pittas, T. Streaming algorithms for high-dimensional robust statistics. In *International Conference on Machine Learning*, pp. 5061–5117. PMLR, 2022.

Dua, D. and Graff, C. Uci machine learning repository, 2017. URL http://archive.ics.uci.edu/ml.

Duchi, J., Hashimoto, T., and Namkoong, H. Distributionally robust losses for latent covariate mixtures. *Operations Research*, 2022.

Duchi, J. C. and Namkoong, H. Learning models with uniform performance via distributionally robust optimization. *The Annals of Statistics*, 49(3):1378–1406, 2021.

Esposito, A., Patacchini, F. S., Schlichting, A., and Slepčev, D. Nonlocal-interaction equation on graphs: gradient flow structure and continuum limit. *Archive for Rational Mechanics and Analysis*, 240(2):699–760, 2021.

Friston, K. The free-energy principle: a unified brain theory? *Nature reviews neuroscience*, 11(2):127–138, 2010.

Frogner, C., Claici, S., Chien, E., and Solomon, J. Incorporating unlabeled data into distributionally robust learning. *arXiv preprint arXiv:1912.07729*, 2019.

Fu, X., Shen, W., Yao, T., and Hou, W. Physical chemistry. *Higher Education, Beijing*, 1990.

Gao, R. and Kleywegt, A. Distributionally robust stochastic optimization with wasserstein distance. *Mathematics of Operations Research*, 2022.

Gao, R., Chen, X., and Kleywegt, A. J. Wasserstein distributionally robust optimization and variation regularization. *Operations Research*, 2022.

Gulrajani, I. and Lopez-Paz, D. In search of lost domain generalization. In *9th International Conference on Learning Representations, ICLR 2021, Virtual Event, Austria, May 3-7, 2021*. OpenReview.net, 2021. URL https://openreview.net/forum?id=lQdXeXDoWtI.

Hu, W., Niu, G., Sato, I., and Sugiyama, M. Does distributionally robust supervised learning give robust classifiers? In *International Conference on Machine Learning*, pp. 2029–2037. PMLR, 2018.

Hu, Z. and Hong, L. J. Kullback-leibler divergence constrained distributionally robust optimization. *Available at Optimization Online*, 1(2):9, 2013.

Huber, P. J. Robust estimation of a location parameter. *Breakthroughs in statistics: Methodology and distribution*, pp. 492–518, 1992.

Iyengar, G., Lam, H., and Wang, T. Hedging against complexity: Distributionally robust optimization with parametric approximation. In *International Conference on Artificial Intelligence and Statistics*, pp. 9976–10011. PMLR, 2023.

Kingma, D. P. and Ba, J. Adam: A method for stochastic optimization. In Bengio, Y. and LeCun, Y. (eds.), *3rd International Conference on Learning Representations, ICLR 2015, San Diego, CA, USA, May 7-9, 2015, Conference Track Proceedings*, 2015. URL http://arxiv.org/abs/1412.6980.

Klivans, A., Kothari, P. K., and Meka, R. Efficient algorithms for outlier-robust regression. In *Conference On Learning Theory*, pp. 1420–1430. PMLR, 2018.

Levina, E. and Bickel, P. J. Maximum likelihood estimation of intrinsic dimension. In *Advances in Neural Information Processing Systems 17 [Neural Information Processing Systems, NIPS 2004, December 13-18, 2004, Vancouver, British Columbia, Canada]*, pp. 777–784, 2004.

Liu, J., Shen, Z., Cui, P., Zhou, L., Kuang, K., and Li, B. Distributionally robust learning with stable adversarial training. *IEEE TKDE*, 2022a.

Liu, J., Wu, J., Li, B., and Cui, P. Distributionally robust optimization with data geometry. In *Advances in Neural Information Processing Systems*, 2022b.

Lunga, D., Prasad, S., Crawford, M. M., and Ersoy, O. Manifold-learning-based feature extraction for classification of hyperspectral data: A review of advances in manifold learning. *IEEE Signal Processing Magazine*, 31 (1):55–66, 2013.

Namkoong, H. and Duchi, J. C. Variance-based regularization with convex objectives. *Advances in neural information processing systems*, 30, 2017.

Narayanan, H. and Mitter, S. K. Sample complexity of testing the manifold hypothesis. In Lafferty, J. D., Williams, C. K. I., Shawe-Taylor, J., Zemel, R. S., and Culotta, A. (eds.), *Advances in Neural Information Processing Systems 23: 24th Annual Conference on Neural Information Processing Systems 2010. Proceedings of a meeting held 6-9 December 2010, Vancouver, British Columbia, Canada*, pp. 1786–1794. Curran Associates, Inc., 2010.

Ozakin, A. and Gray, A. G. Submanifold density estimation. In Bengio, Y., Schuurmans, D., Lafferty, J. D., Williams, C. K. I., and Culotta, A. (eds.), *Advances in Neural Information Processing Systems 22: 23rd Annual Conference on Neural Information Processing Systems 2009. Proceedings of a meeting held 7-10 December 2009, Vancouver, British Columbia, Canada*, pp. 1375–1382. Curran Associates, Inc., 2009.

Pope, P., Zhu, C., Abdelkader, A., Goldblum, M., and Goldstein, T. The intrinsic dimension of images and its impact on learning. *ICLR*, 2021.

Reichl, L. E. A modern course in statistical physics, 1999.

Roweis, S. T. and Saul, L. K. Nonlinear dimensionality reduction by locally linear embedding. *Science*, 290 (5500):2323–2326, 2000. doi: 10.1126/science.290.5500.2323. URL https://www.science.org/doi/abs/10.1126/science.290.5500.2323.

Sinha, A., Namkoong, H., and Duchi, J. C. Certifying some distributional robustness with principled adversarial training. In *6th International Conference on Learning Representations, ICLR 2018, Vancouver, BC, Canada, April 30 - May 3, 2018, Conference Track Proceedings*. OpenReview.net, 2018. URL https://openreview.net/forum?id=Hk6kPgZA-.

Słowik, A. and Bottou, L. On distributionally robust optimization and data rebalancing. In *International Conference on Artificial Intelligence and Statistics*, pp. 1283–1297. PMLR, 2022.

Staib, M. and Jegelka, S. Distributionally robust optimization and generalization in kernel methods. *Advances in Neural Information Processing Systems*, 32, 2019.

Villani, C. Topics in optimal transportation. 58, 2021.

Wang, J., Gao, R., and Xie, Y. Sinkhorn distributionally robust optimization. *arXiv preprint arXiv:2109.11926*, 2021.

Wang, M., Yu, L., Zheng, D., Gan, Q., Gai, Y., Ye, Z., Li, M., Zhou, J., Huang, Q., Ma, C., Huang, Z., Guo, Q., Zhang, H., Lin, H., Zhao, J., Li, J., Smola, A. J., and Zhang, Z. Deep graph library: Towards efficient and scalable deep learning on graphs. *CoRR*, abs/1909.01315, 2019. URL http://arxiv.org/abs/1909.01315.

Zeng, Y. and Lam, H. Generalization bounds with minimal dependency on hypothesis class via distributionally robust optimization. *Advances in Neural Information Processing Systems*, 35:27576–27590, 2022.

Zhai, R., Dan, C., Kolter, Z., and Ravikumar, P. Doro: Distributional and outlier robust optimization. In *International Conference on Machine Learning*, pp. 12345–12355. PMLR, 2021.

A. Implementation

For our GCDRO, G_N is constructed as a k-nearest neighbor (kNN) graph from training data *once and for all* ***only at the initialization step***. For large-scale datasets, we use NN-Descent to estimate the kNN graph with an almost linear complexity of $\mathcal{O}(\mathbf{N^{1.14}})$. Since the sample weights are transferred along the edges of the graph, the simulation of gradient flow can be implemented similarly to message propagation with DGL package (Wang et al., 2019), which ***scales linearly with sample size*** and enjoys *parallelization by GPU*. The implementation above ensures the adaptability to large-scale data.

B. Improvements of our work.

In Section 2, we have introduced the typical DRO methods in detail and demonstrated the over-pessimism problem. Here we compare our work with several DRO works and clarify their differences.
(1) With MMD-DRO: MMD-DRO (Staib & Jegelka, 2019) also has a quadratic term in its dual reformulation, while Staib & Jegelka (2019) focuses on the equivalence between MMD-DRO and Hilbert norms and there is no efficient or applicable algorithm yet. Further, it remains the risk objective unchanged (the quadratic term is from MMD distance) and just uses the Gaussian RBF kernel. Our work firstly incorporates the data geometry into the design of the calibration term and demonstrates its relationship with Helmholtz free energy, and we propose an applicable algorithm that could be used under deep models.
(2) With GDRO: GDRO (Liu et al., 2022b) uses the discrete geometric Wasserstein distance to build the uncertainty set, and intuitively demonstrates its superiority. Our work theoretically analyzes the over-pessimism problem and attributes the cause of over-pessimism to the excessive focus on noisy samples in DRO. And for the risk objective function, our work further introduces the graph total variation term to mitigate the effects of noisy samples, which is theoretically justified and empirically verified. From our results, GDRO is heavily affected by noisy samples, while our GCDRO has a much better performance. Further, this work relates the newly-proposed risk objective to the Helmholtz free energy and unifies some typical DRO methods into it, which is a new perspective to view DRO methods and could inspire future research.
(3) With DORO: DORO (Zhai et al., 2021) proposes to dismiss data samples with the top losses and then performs DRO, and we compare with it in our experiments. Theoretically, this method relies on the implicit assumption that noisy samples must have larger prediction errors than hard clean samples. However, this assumption does not always hold, and as shown in our experiments, it has some effects but does not work very well.

C. Why uses kNN graph?

Manifold Assumption. The data manifold hypothesis indicates that high-dimensional data often lies in an unknown lower-dimensional manifold embedded in ambient space (Roweis & Saul, 2000; Belkin & Niyogi, 2003; Levina & Bickel, 2004; Lunga et al., 2013; Brown et al., 2022) and is supported by strong evidence. From a theoretical perspective, Ozakin & Gray (2009); Narayanan & Mitter (2010) prove that when such hypothesis holds, manifold learning and density estimation scale exponentially with the *low intrinsic* dimension, but otherwise scale exponentially with the *high ambient* dimension (Cacoullos, 1964). Therefore, as Brown et al. (2022) point out, one most plausible explanation for the success of machine learning methods on real-world data is the existence of such lower intrinsic dimension, which enables learning on datasets of fairly reasonable size, which is empirically verified by Pope et al. (2021). Also, for two of the real-world tabular datasets used in this work, we visualize their 3-dimensional manifolds and calculate their intrinsic dimensions in Figure 3.

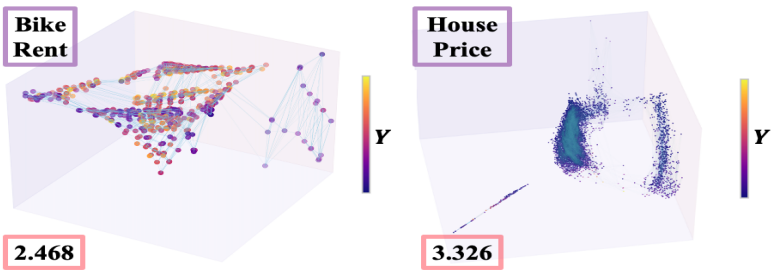

Figure 3: Visualization of the 3-dimensional manifold of the tabular datasets, and the numbers in the lower left represent the intrinsic dimension according to (Levina & Bickel, 2004)

Our GCDRO algorithm uses an input-weighted graph G_N to approximate the data manifold. The kNN graph is a fundamental and basic way to represent the data structure, and manifold learning is an area with intensive research. We have to clarify that manifold learning is not the focus of this paper, which takes the data structure G_N as input to design a DRO objective and optimization algorithm that incorporates data geometric information for more reasonable worst-case distribution. Notably, our GCDRO achieves significant performance in the experiments even with the simple kNN representation of data structure. It proves that this direction for geometric-aware DROs is promising, and our proposed method could efficiently leverage the geometric properties encoded in the input graph to mitigate the effects of harmful data points (note that no target information is leaked into G_N). Actually, our GCDRO is compatible with any manifold learning or graph learning method. We do believe that a more accurate estimated data structure with advanced manifold learning algorithms will further boost the performance of GCDRO, and we leave this to future work.

Not Sensitive to k. For the house pricing dataset, we plot the results of our GCDRO with varying ks in Figure 4. We could see that the performance of our algorithm is not affected much.

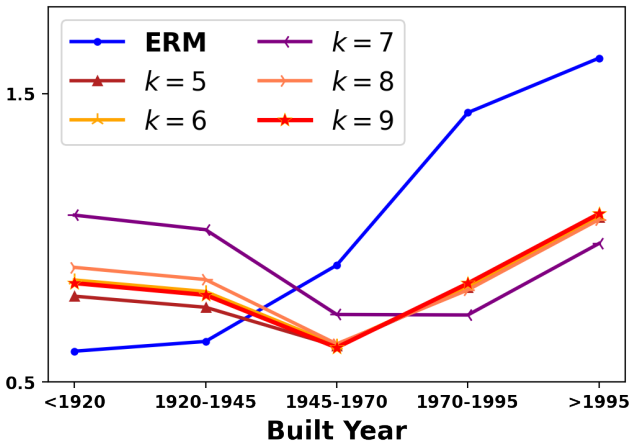

Figure 4: Results with varying k.

D. Experimental Details

Model & Loss function. For simulation data, we use linear models for all methods. For real-world data, we use two-layer MLPs for all methods.

Optimizer. For all experiments, we use Adam with a learning rate of $1e-3$ in PyTorch for all methods.

Hyper-parameters. For KLDRO, WDRO and χ^2-DRO, we grid search the radius of the uncertainty set within the range of $[1e-3, 2e2]$, and we select the best hyper-parameters according to their testing performances. For GDRO, we grid search the number of gradient flow steps within the range of $[1e2, 2e3]$, the parameter $\beta \in [1, 20]$ and we select the best hyper-parameters according to its testing performances. For DORO, we set the noisy ratio to the ground-truth value for the simulation data, and we grid search the ratio of noisy points within the range of $[1e-2, 5e-1]$ for the real-world data. For HRDRO, we use L_1 loss as proposed in (Bennouna & Van Parys, 2022) and grid search $\epsilon \in [1e-3, 1]$. For GCDRO, we grid search the number of gradient flow steps within the range of $[1e2, 2e3]$, $\beta \in [1, 20]$ and $\alpha \in [1e-1, 1e1]$. We select the best hyper-parameters according to their testing performances.

Note that in our experiments, we found that model selection without domain information in the validation set is very hard, which is also verified by (Zhai et al., 2021; Gulrajani & Lopez-Paz, 2021). And we believe this is still an open problem and is fairly non-trivial.

E. Examples on Label Noise

Theorem E.1. *Assume that the training data is a mixture of n_c clean samples $\{x_c^{(i)}, y_c^{(i)}\}$ drawn from distribution $P_c(X, Y)$ and n_o noisy samples $\{x_o^{(i)}, y_o^{(i)}\}$ drawn from distribution $P_o(X, Y)$. Consider a linear data generation process, i.e.*

$Y = kX + \xi$ and $\xi \perp X, \mathbb{E}[\xi] = 0$ and $\mathbb{E}[\xi^2]$ is finite (abbr. σ^2). The regression model is parameterized as $f(x) = \theta \cdot x$ and trained with Weighted Least Square estimation:

$$\hat{\theta} = \arg\min_{\theta} \sum_{i=1}^{n_c} w_c^{(i)} \|(y_c^{(i)} - \theta \cdot x_c^{(i)})\|^2 + \sum_{i=1}^{n_o} w_o^{(i)} \|(y_o^{(i)} - \theta \cdot x_o^{(i)})\|^2. \tag{10}$$

$$s.t. \quad \sum_{i=1}^{n_c} w_c^{(i)} + \sum_{i=1}^{n_o} w_o^{(i)} = 1, \tag{11}$$

where $w_c^{(i)}, w_o^{(i)} \geq 0$ are weights on clean and noisy samples respectively, and $\sigma_c^2 < \sigma_o^2$. Then the variance of the least square estimate $\hat{\theta}$ is given by:

$$Var[\hat{\theta}|X_D] = \frac{\sum_{i=1}^{n_c} (w_c^{(i)})^2 (x_c^{(i)})^2 \sigma_c^2 + \sum_{i=1}^{n_o} (w_o^{(i)})^2 (x_o^{(i)})^2 \sigma_o^2}{\left[\sum_{i=1}^{n_c} w_c^{(i)} (x_c^{(i)})^2 + \sum_{i=1}^{n_o} w_o^{(i)} (x_o^{(i)})^2\right]^2}, \tag{12}$$

where $X_D = \{x_c^{(i)}\} \cup \{x_o^{(i)}\}$ is the sampled covariates in the dataset. Further, the variance of the estimator $\hat{\theta}$ achieves the minimum if and only if:

$$\forall 1 \leq i \leq n_c, 1 \leq j \leq n_o, \quad \gamma(i,j) = w_o^{(j)} / w_c^{(i)} = \sigma_c^2 / \sigma_o^2, \tag{13}$$

where $\gamma(i,j)$ denotes the sample weight ratio between i and j.

The theorem is a direct corollary of the following lemma.

Lemma E.2. *Assume that the training data contains n samples $\{x^{(i)}, y^{(i)}\}$. Consider a linear data generation process with heterogeneous noise, i.e. $y^{(i)} = kx^{(i)} + \xi_i$ with $\xi_i \perp X, \mathbb{E}[\xi_i] = 0$, and $\mathbb{E}[\xi_i^2]$ is finite. The regression model is parameterized as $f(x) = \theta \cdot x$ and trained with Weighted Least Square estimation:*

$$\hat{\theta} = \arg\min_{\theta} \sum_{i=1}^{n} w^{(i)} \|(y^{(i)} - \theta \cdot x^{(i)})\|^2. \tag{14}$$

$$s.t. \quad \sum_{i=1}^{n} w^{(i)} = 1, \tag{15}$$

where $w^{(i)} \geq 0$ are sample weights. Then the variance of the least square estimate $\hat{\theta}$ is given by:

$$Var[\hat{\theta}|X_D] = \frac{\sum_{i=1}^{n} (w^{(i)})^2 (x^{(i)})^2 \sigma_i^2}{\left[\sum_{i=1}^{n} w^{(i)} (x^{(i)})^2\right]^2}, \tag{16}$$

where $X_D = \{x^{(i)}\}$ is the sampled covariates in the dataset. Further, the variance of the estimator $\hat{\theta}$ achieves the minimum if and only if:

$$\forall 1 \leq i \leq n, 1 \leq j \leq n, \quad w^{(i)} \sigma_i^2 = w^{(j)} \sigma_j^2. \tag{17}$$

Proof. According to the heterogeneous noise distribution, let $y^{(i)} = x^{(i)} + \epsilon_i$, where $\epsilon_i \sim \mathcal{N}(0, \sigma_i^2)$. The least square estimation of $\hat{\theta}$ is given by:

$$\hat{\theta} = k + \frac{\sum_{i=1}^{n} w^{(i)} x^{(i)} \epsilon_i}{\sum_{i=1}^{n} w^{(i)} (x^{(i)})^2}. \tag{18}$$

Since $\mathbb{E}[\hat{\theta}|X_D] = k$, we have

$$\text{Var}[\hat{\theta}|X_D] = \mathbb{E}\left|\frac{\sum_{i=1}^{n} w^{(i)} x^{(i)} \epsilon_i}{\sum_{i=1}^{n} w^{(i)} (x^{(i)})^2}\right|^2 \tag{19}$$

$$= \frac{\sum_{i=1}^{n} (w^{(i)})^2 (x^{(i)})^2 \sigma_i^2}{\left[\sum_{i=1}^{n} w^{(i)} (x^{(i)})^2\right]^2}. \tag{20}$$

Next, we solve the minimum of Eq.16 w.r.t. sample weights $w^{(i)}$. Let $\alpha_i = w^{(i)}(x^{(i)})^2$. We could formulate the variance in Eq.16 as a function of $\alpha = (\alpha_1, ..., \alpha_n)$:

$$V(\alpha) = \frac{\sum_{i=1}^n \alpha_i^2 \sigma_i^2 / (x^{(i)})^2}{\left(\sum_{i=1}^n \alpha_i\right)^2}. \tag{21}$$

Since $V(\lambda\alpha) = V(\alpha)$ for any $\lambda > 0$, we could assume $\sum_{i=1}^n \alpha_i = 1$ without loss of generality. Then the minimization of $V(\alpha)$ is equivalent to:

$$\min_{\alpha} \quad V(\alpha) \left(= \sum_{i=1}^n \alpha_i^2 \sigma_i^2 / (x^{(i)})^2 \right) \tag{22}$$

$$s.t. \quad \sum_{i=1}^n \alpha_i = 1. \tag{23}$$

The first-order KKT condition gives:

$$\exists C, \forall 1 \le i \le n, \quad \alpha_i^* = C(x^{(i)})^2 / \sigma_i^2, \tag{24}$$

from which we can solve:

$$\alpha_i^* = \frac{(x^{(i)})^2 / \sigma_i^2}{\sum_{j=1}^n (x^{(j)})^2 / \sigma_j^2}. \tag{25}$$

Since $\nabla_\alpha^2 V(\alpha) = diag\left[2\sigma_1^2/(x^{(1)})^2, ..., 2\sigma_n^2/(x^{(n)})^2\right]$ is always positive definite, Eq.25 minimizes $V(\alpha)$. Correspondingly $w^{(i)} \propto 1/\sigma_i^2$, which finishes the proof. □

F. Proofs

F.1. Proof of Proposition 2.1

Proof. (1) For KL-divergence as the distance function, we have the following optimization problem under finite samples.

$$\min_{\theta \in \Theta, \lambda \ge 0} \sup_{\mathbf{p} \in \Delta_n} \left\{ \sum_{i=1}^n p_i \ell(f_\theta(x_i), y_i) - \lambda \sum_{i=1}^n p_i \log p_i + \lambda(\epsilon - \log n) \right\}, \tag{26}$$

Solve the inner supremum problem, and the worst-case distribution is like:

$$p_i = \exp\left(\frac{\ell_i - \eta}{\lambda} - 1\right), \ \eta(\ell) = \lambda \log \lambda + \lambda \log \left(\sum_{i=1}^n \exp\left(\frac{\ell_i}{\lambda} - 1\right) \right), \tag{27}$$

and the objective function becomes:

$$\min_{\theta \in \Theta, \lambda \ge 0} \lambda \log \left(\sum_{i=1}^n \exp\left(\frac{\ell(f_\theta(x_i), y_i))}{\lambda} \right) \right) + \lambda(\epsilon + \log \lambda - \log n). \tag{28}$$

And we could compare the sample weights of different samples as:

$$\frac{p_i}{p_j} = \exp\left(\frac{\ell_i - \ell_j}{\lambda}\right). \tag{29}$$

(2) For χ^2-divergence which is defined as $f(x) = (x-1)^2$, we have the following optimization problem.

$$\min_{\theta \in \Theta, \lambda \ge 0} \sup_{\mathbf{p} \in \Delta_n} \left\{ \sum_{i=1}^n p_i \ell(f_\theta(x_i), y_i) + \lambda\epsilon - \frac{\lambda}{n} \sum_{i=1}^n (np_i - 1)^2 \right\}. \tag{30}$$

Solve the inner supremum problem, and we have the worst-case distribution like:

$$p_i = \frac{1}{\lambda n}(\ell_i + \lambda - \eta)_+, \tag{31}$$

and the objective function becomes:

$$\min_{\theta\in\Theta,\lambda\geq 0,\eta\in\mathbb{R}} \sum_{i=1}^{n} \frac{1}{2\lambda}(\ell_i + \lambda - \eta)_+^2 + \lambda\epsilon + \eta - \frac{\lambda}{2}. \tag{32}$$

And we could compare the sample weights of different samples as:

$$\frac{p_i}{p_j} = \frac{(\ell_i + \lambda - \eta)_+}{(\ell_j + \lambda - \eta)_+}, \tag{33}$$

if $p_j > 0$.

(3) For Maximal Mean Discrepancy (MMD) distance, we have the following optimization problem:

$$\sup_{\mathbf{p}} \left\{ \sum_{i=1}^{n} p_i \ell_i + \lambda\epsilon - \lambda(\mathbf{p} - \frac{\mathbf{1}}{\mathbf{n}})^{\mathbf{T}} \mathbf{K} (\mathbf{p} - \frac{\mathbf{1}}{\mathbf{n}}) \right\} \tag{34}$$

$$\text{s.t.} \quad \sum_{i=1}^{n} p_i = 1 \tag{35}$$

$$p_i \geq 0, \text{for } i = 1, \ldots, n \tag{36}$$

Solve the inner supremum problem, and we have the worst-case distribution like:

$$p^* = \frac{1}{2\lambda} K^{-1}(\ell - \eta + \frac{2\lambda}{n} K\mathbf{1})_+, \tag{37}$$

and the objective function becomes:

$$\min_{\theta\in\Theta,\lambda\geq 0,\eta\in\mathbb{R}} \frac{1}{4\lambda}(\ell + \frac{2\lambda}{n} K\mathbf{1} - \eta)_+ K^{-1} (\ell + \frac{2\lambda}{n} K\mathbf{1} - \eta)_+ + \lambda\epsilon + \eta - \frac{\lambda}{n^2}\mathbf{1}^T K\mathbf{1}. \tag{38}$$

□

F.2. Proof of Proposition 3.1

Proof. The proof of KL-DRO, χ^2-DRO and MMD DRO is obtained from the proof of Proposition 2.1. For marginal DRO, it is easy to prove following Duchi et al. (2022). For GDRO, it is easy to prove following Liu et al. (2022b). □

F.3. Proof of Proposition 3.2

Proof. The proof is based on the Theorem 5 in (Chow et al., 2017). From (Chow et al., 2017), we have

$$\mathcal{R}_N(q^\infty) - \mathcal{R}_N(q(t)) \leq e^{-Ct}(\mathcal{R}_N(q^\infty) - \mathcal{R}_N(q^0)). \tag{39}$$

Furthermore,

$$C := 2m\lambda_{\text{sec}}(\hat{L})\lambda_{\min}(\nabla^2\mathcal{R}_N)\frac{1}{(r+1)^2} > 0, \tag{40}$$

and

$$r = \sqrt{2}k \max_{(i,j)\in E} w_{ij} \frac{\|\text{Hess}\mathcal{R}_N\|_1}{\lambda_{\min}(\text{Hess}\mathcal{R}_N)^{1.5}} \frac{1-m}{m^2} \frac{\lambda_{\max}(\hat{L})}{\lambda_{\text{sec}}(\hat{L})^2} \sqrt{\mathcal{R}_N(q^0) - \mathcal{R}_N(q^\infty)}, \tag{41}$$

where k denotes the number of neighbors in the kNN graph, $\hat{L}$ is the graph Laplacian matrix, $\lambda_{\text{sec}}, \lambda_{\min}$ are the second smallest and smallest eigenvalue, and

$$\|\text{Hess}\mathcal{R}_N\|_1 = \sup_{q\in\mathscr{P}(G_N)} \|\text{Hess}\mathcal{R}_N(q)\|_1, \quad \lambda_{\min}(\text{Hess}\mathcal{R}_N) = \min_{q\in\mathscr{P}(G_N)} \lambda_{\min}(\text{Hess}\mathcal{R}_N(q)), \tag{42}$$

and

$$m = \frac{1}{2}\left(\frac{1}{(1+2M)^{\frac{1}{\beta}}}\right)^{N-2} \min\left\{\frac{1}{(1+2M)^{\frac{1}{\beta}}}, \frac{1}{N}\right\}. \tag{43}$$

Then denote the real worst-case distribution within the $\epsilon(\theta)$-radius discrete Geometric Wasserstein-ball as q^*, that is,

$$q^* = \arg \sup_{q:\mathcal{GW}^2_{G_N}(\hat{P}_{tr},q)\leq\epsilon(\theta)} \mathcal{R}_N(\theta, q), \tag{44}$$

and we have

$$\mathcal{R}_N(q^\infty) - \mathcal{R}_N(q^*) + \mathcal{R}_N(q^*) - \mathcal{R}_N(q(t)) \leq e^{-Ct}(\mathcal{R}_N(q^\infty) - \mathcal{R}_N(q^*) + \mathcal{R}_N(q^*) - \mathcal{R}_N(q^0)). \tag{45}$$

Therefore, we have

$$\mathcal{R}_N(q^*) - \mathcal{R}_N(q(t)) \leq e^{-Ct}(\mathcal{R}_N(q^*) - \mathcal{R}_N(q^0)) - (1-e^{-Ct})(\mathcal{R}_N(q^\infty) - \mathcal{R}_N(q^*)), \tag{46}$$

and

$$\frac{\mathcal{R}_N(q^*) - \mathcal{R}_N(q(t))}{\mathcal{R}_N(q^*) - \mathcal{R}_N(q^0)} \leq e^{-Ct} - (1-e^{-Ct})\frac{\mathcal{R}_N(q^\infty) - \mathcal{R}_N(q^*)}{\mathcal{R}_N(q^*) - \mathcal{R}_N(q^0)} < e^{-Ct}. \tag{47}$$

□

F.4. Proof of Proposition 3.3

Proof. Denote $\delta = \ell_i^{\text{noisy}} - \ell_i$. First, it is easy to prove that (through some simple calculation):

$$\xi_{\text{GDRO}}(i,j) = \frac{\delta}{\beta}, \tag{48}$$

$$\xi_{\text{GCDRO}}(i,j) = \frac{1}{\beta}(\delta - \alpha \cdot h), \tag{49}$$

where

$$\begin{aligned} h &= \delta^2 \cdot (\sum_{k\in N(i)} \tilde{q}_k^* w_{ik}) + \delta \cdot (\sum_{k\in N(i)} 2\tilde{q}_k^* w_{ik}(\ell_i - \ell_k)) + \sum_{k\in N(i)} (\tilde{q}_k^* - q_k^*) w_{ik}(\ell_i - \ell_k)^2 - \sum_{k\in N(j)} (\tilde{q}_k^* - q_k^*) w_{jk}(\ell_k - \ell_j)^2 \\ &= A\delta^2 + 2B\delta + C. \end{aligned} \tag{50}$$

Therefore, when

$$\delta \geq \delta_{\min} := \begin{cases} -\frac{B}{A} + \sqrt{(\frac{B}{A})^2 - \frac{C}{A}} & \text{if } B^2 - AC \geq 0, \\ 0, & \text{otherwise.} \end{cases} \tag{51}$$

we have $h > 0$, which gives that for any $\alpha > 0$, $\xi_{\text{GCDRO}}(i,j) < \xi_{\text{GDRO}}(i,j)$.

Furthermore, when $\delta - \alpha h < 0$, i.e. $\alpha > 1/(A\delta + 2B + \frac{C}{\delta})$, we have $\xi_{\text{GCDRO}}(i,j) < 0$.

□